The ACE-MAESTRO instrument on SCISAT: description, performance, and preliminary results

C. Thomas McElroy,[1,2,*] Caroline R. Nowlan,[2] James R. Drummond,[2,3] Peter F. Bernath,[4,5] David V. Barton,[1] Denis G. Dufour,[2] Clive Midwinter,[1,2] Robert B. Hall,[1] Akira Ogyu,[1] Aaron Ullberg,[1] David I. Wardle,[1] Jay Kar,[2] Jason Zou,[2] Florian Nichitiu,[2] Chris D. Boone,[4] Kaley A. Walker,[2,4] and Neil Rowlands[6]

[1]Environment Canada, 4905 Dufferin Street, Toronto, Ontario, Canada M3H 5T4
[2]Department of Physics, University of Toronto, 60 St. George Street, Toronto, Ontario, Canada M5S 1A7
[3]Department of Physics and Atmospheric Science, Dalhousie University, Halifax, Nova Scotia, Canada B3H 3J5
[4]Department of Chemistry, University of Waterloo, 200 University Avenue West, Waterloo, Ontario, Canada N2L 3G1
[5]Department of Chemistry, University of York, Heslington, York, UK YO10 5DD
[6]COM DEV Ltd., 303 Terry Fox Drive, Ottawa, Ontario, Canada K2K 3J1

*Corresponding author: tom.mcelroy@ec.gc.ca

Received 6 November 2006; revised 20 February 2007; accepted 21 February 2007; posted 21 February 2007 (Doc. ID 76743); published 20 June 2007

The Measurement of Aerosol Extinction in the Stratosphere and Troposphere Retrieved by Occultation (MAESTRO) instrument on the SCISAT satellite is a simple, compact spectrophotometer for the measurement of atmospheric extinction, ozone, nitrogen dioxide, and other trace gases in the stratosphere and upper troposphere as part of the Atmospheric Chemistry Experiment (ACE) mission. We provide an overview of the instrument from requirements to realization, including optical design, prelaunch and on-orbit performance, and a preliminary examination of retrievals of ozone and NO_2. © 2007 Optical Society of America

OCIS codes: 010.1280, 010.4950.

1. Introduction

The Atmospheric Chemistry Experiment (ACE) mission on the SCISAT satellite is designed to examine the composition of the Earth's atmosphere from space, with special emphasis on the middle-atmosphere ozone distribution and related trace gases in the Arctic. SCISAT is Canada's first scientific satellite for atmospheric sounding in over 30 years and was launched on 12 August 2003. The ACE payload comprises two instruments: the Fourier transform spectrometer (ACE-FTS; hereinafter referred to as the FTS), described in Bernath *et al.* [1], which operates in the infrared (IR) from 750 to 4400 cm^{-1} (2.3–13.3 μm) with an unapodized spectral resolution of 0.02 cm^{-1}, and the Measurement of Aerosol Extinction in the Stratosphere and Troposphere Retrieved by Occultation instrument (ACE-MAESTRO; hereinafter referred to as MAESTRO), which is a dual, diode-array spectrometer measuring in the UV-visible-near-infrared (UV-VIS-NIR) spectral regions with a nominal wavelength range between 285 and 1015 nm (400 and 1010 nm for its primary measurement mode of solar occultation). The FTS instrument also contains two solar imagers consisting of 128 × 128 pixel arrays [2]. The VIS imager array operates at 527.1 nm with a full width at half-maximum (FWHM) filter bandwidth of 13.3 nm, and the NIR imager operates at 1020.6 nm with a bandwidth of 19.4 nm.

Both the FTS and MAESTRO make measurements in the solar occultation mode and share a common suntracker and optical boresight. Therefore, they examine almost the same slant column of air, albeit with different fields of view (FOVs), and with only a slight difference resulting from differential refractive effects and a relatively small 0.02° (1 km tangent altitude)

0003-6935/07/204341-16$15.00/0

pointing alignment offset between the centers of the MAESTRO and FTS FOVs. A solar occultation measurement occurs at the point during the orbit when the satellite–Sun vector intersects the atmosphere, and spectral measurements of the extinction of solar radiation can be made for determining profiles of atmospheric constituents. Solar occultation provides a high signal-to-noise ratio and high-vertical resolution. The high-vertical resolution is possible due to the large geometric weighting of the absorption in the tangent layer (the layer of the solar ray's closest approach to the Earth's surface) relative to that of the layers above in a spherical atmosphere. Approximately 15 sunrise and 15 sunset measurements are possible each day from SCISAT's circular 650 km and 74° inclination orbit. In addition to the primary solar occultation measurement mode, MAESTRO also has the capability of making measurements of solar radiation scattered back into space by the Earth's atmosphere.

This paper describes the MAESTRO instrument, beginning with the science requirements, and then discusses the design, testing, and characterization of the instrument. The current operational data processing algorithms are also presented, and sample retrieved ozone and NO_2 profiles from solar occultation are shown.

2. Scientific Contribution

A full investigation of the global ozone budget requires detailed species measurements (including O_3, H_2O, NO, NO_2, N_2O_5, HNO_3, HNO_4, HCl, $ClNO_3$, and ClO) and measurements of aerosol extinction in the VIS, NIR, and mid-IR in order to derive the composition, size, and density of aerosols and polar stratospheric clouds (see, for example, World Meteorological Organization [3]). In combination with atmospheric models, measurements of these species can be used to provide valuable insights into ozone chemistry and dynamics, differences between the Arctic and Antarctic ozone distributions, the chlorine budget, and wintertime denitrification. Although the FTS is able to measure aerosol extinction in the mid-IR and as many as 33 trace gases, when the FTS was originally selected for the SCISAT payload in 1998, it was recognized that the capabilities of the ACE mission could be greatly enhanced by the addition of a UV-VIS-NIR spectrometer that would extend the wavelength range of the ACE measurements, particularly for aerosol extinction measurements, as well as providing some scientific and mission redundancy. With this in mind, MAESTRO was selected as an addition to ACE in early 2000, just over 3 years before the launch.

The overall mission objectives for the ACE mission, as described by Bernath *et al.* [1], are to (1) better quantify the chemical and dynamical processes affecting the stratospheric and upper tropospheric ozone distribution, particularly in the Arctic; (2) explore the relationship between atmospheric chemistry and climate change; (3) examine the effects of biomass burning on the free troposphere; and (4) determine aerosol and cloud properties to reduce uncertainties in quantifying their effects on the global energy balance. Examining the ozone budget is the highest priority for the ACE mission.

The primary scientific enhancements to the ACE mission resulting from the addition of MAESTRO are (1) the provision of moderate-resolution, wavelength-dependent aerosol extinction data in the 400–1010 nm wavelength range; (2) the determination of ozone and NO_2 concentration profiles with higher precision and vertical resolution than the FTS data can provide; and (3) improved traceability of ozone measurements to other UV-VIS-NIR satellite measurements, such as those from the Stratospheric Aerosol and Gas Experiment III (SAGE III) [4] and Polar Ozone and Aerosol Measurement III (POAM III) [5] instruments.

These enhancements are made possible from MAESTRO solar occultation spectral measurements in the UV-VIS-NIR, where there are strong absorption features due to ozone, NO_2, H_2O, and O_2, as well as scattering by aerosols and molecules (Rayleigh scattering). Other weakly absorbing molecules such as the O_2–O_2 dimer also absorb in the MAESTRO measurement range. From these extinction data, molecular species concentrations can be retrieved, and the residual extinction remaining after accounting for the molecular absorption and scattering can be taken as representative of aerosol attenuation. This UV-VIS-NIR aerosol extinction is required to properly quantify the properties of atmospheric aerosols (e.g., particle densities and size distribution) and to estimate the aerosol surface area in the same atmospheric regions where composition measurements are made.

MAESTRO also has a secondary measurement mode for observing sunlight scattered back into space from the atmosphere below the satellite, permitting the global mapping of ozone and NO_2 total column amounts. Depending on the season, atmospheric conditions, and location, SO_2, OClO, and BrO may also be observable in this mode.

The specific science goals for MAESTRO are essentially derived from the original desire of the ACE team to extend the wavelength range of the mission for aerosol extinction measurements in the UV-VIS-NIR. By virtue of these additional measurements in this wavelength range and the instrument's design, MAESTRO is also able to contribute in other ways to the ACE science goals. Mission and scientific redundancy is provided in occultation measurements of ozone and several other species. MAESTRO also provides measurements with enhanced vertical resolution (~1–2 km) over the FTS vertical resolution (~4 km), which is important for improving the modeling of chemistry and dynamics of air parcels, and in particular for studying polar stratospheric clouds, which are highly structured in the vertical. These requirements and/or contributions (extended wavelength coverage for aerosol extinction, scientific and/or mission redundancy, and higher-vertical resolution) established the following measurement goals: High-vertical-resolution measurements of aero-

sol optical depth (OD) with accuracies of 0.01 OD (8–10 km) and 0.001 OD (10–50 km), and aerosol extinction wavelength-dependence accuracy of 0.005 OD per 100 nm; high-vertical-resolution ozone profiles with accuracies of 15% (8–10 km), 10% (10–20 km), and 3% (20–50 km) (assuming a midlatitude profile); and high-vertical-resolution NO_2 profiles with accuracies of 25% (8–10 km), 15% (10–20 km), 10% (20–40 km), and 15% (40–50 km) (assuming a midlatitude profile). Additional species (H_2O, SO_2, OClO, BrO) may be observable in occultation or backscatter in addition to the primary products of ozone, NO_2, and aerosol extinction.

To our knowledge, this is the first time an instrument measuring in the UV-VIS-NIR and an instrument measuring in the mid-IR have been placed on the same spacecraft to view a nearly identical beam of solar radiation from space. As such, the direct comparison of results from MAESTRO and the FTS is of particular scientific interest. These simultaneous observations should lead to improvements in the understanding of the spectroscopy of molecules measured by both instruments and the retrieval methodologies employed. This has direct application to understanding the relationships between measurements from other instruments made using different spectroscopic techniques, such as between the HALogen Occultation Experiment [6] (HALOE), which measures in the IR, and SAGE III, which measures in the UV-VIS-NIR. In addition to providing colocated trace gas and aerosol measurements, this coalignment also allows MAESTRO data analysis to use the tangent pointing and pressure-temperature profiles derived by the FTS CO_2 retrievals [7].

3. MAESTRO Instrument

A. Spectrometer

MAESTRO comprises two independent diode-array spectrometers. One spectrometer measures UV and visible spectra from 285 to 565 nm with a spectral resolution of approximately 1.5 nm, while the second measures VIS and NIR spectra from 515 to 1015 nm with a resolution of approximately 2 nm. These spectrometers will be referred to as the UV and VIS spectrometers, respectively. The main features of MAESTRO, including the properties of the two spectrometers, are summarized in Table 1. While the nominal wavelength range of measurements is 285–1015 nm, the wavelength range that can be calibrated on-orbit in occultation by the matching of solar Fraunhofer features in observed spectra to their known wavelengths is smaller (400–545 nm for the UV spectrometer and 520–1010 nm for the VIS) and is also listed in Table 1. These wavelength-calibration limits depend on the availability of sufficient signal to noise as a function of wavelength, and the occurrence of Fraunhofer lines that can be used for wavelength-pixel matching. Wavelengths past these limits are extrapolated. The above limits are for occultation spectra; backscatter spectra wavelength calibration in the UV can be extended below 300 nm.

Each individual spectrometer is relatively simple and small, consisting of only a lens, slit, concave holographic grating, and photodiode array detector. In solar occultation mode, the two spectrometers are illuminated by light from two separate, folded three-mirror telescopes coupled by beam splitters. The entire MAESTRO instrument is approximately a 0.5 m cube, weighs ~8 kg, and consumes 14 W peak power. Figure 1 shows a photograph of the MAESTRO instrument, labeled with the locations of its solar and backscatter ports. A schematic of the instrument's optical design is shown in Fig. 2. The spectrometer design draws heavily on heritage from the Meteorological Service of Canada's SunPhotoSpectrometer (SPS), which was developed for flight on the Space Shuttle in 1992 and used extensively as part of the NASA ER-2 stratospheric chemistry research program in the 1990s as the Composition and Photodissociative Flux Measurement (CPFM) instrument [8,9].

Table 1. Main Characteristics of the ACE-MAESTRO Instrument

	Spectrometer	
	UV	VIS
Nominal wavelength range	285–565 nm	515–1015 nm
Calibrated wavelength range in occultation	400–545 nm (pixels 463–954)	520–1010 nm (pixels 21–1010)
Spectral resolution	~1.5 nm	~2 nm
Pixel spacing	~0.3 nm	~0.5 nm
Main sources of extinction	O_3, NO_2, aerosol and molecular scattering	O_3, O_2, O_2–O_2, H_2O, aerosol and molecular scattering
Secondary sources of extinction	SO_2, OClO, BrO	NO_2
SCISAT orbit	circular, 650 km altitude, 74° inclination	
Instrument FOV	~1.2 km (elevation) × 25 km (azimuth) (at 22 km tangent)	
Observation modes	Solar occultation Nadir backscatter	
Detectors	1024 pixel, Reticon photodiode array	
Gratings	Concave holographic, 94 mm focal length	
Signal to noise	~1000–3000 (high Sun)	

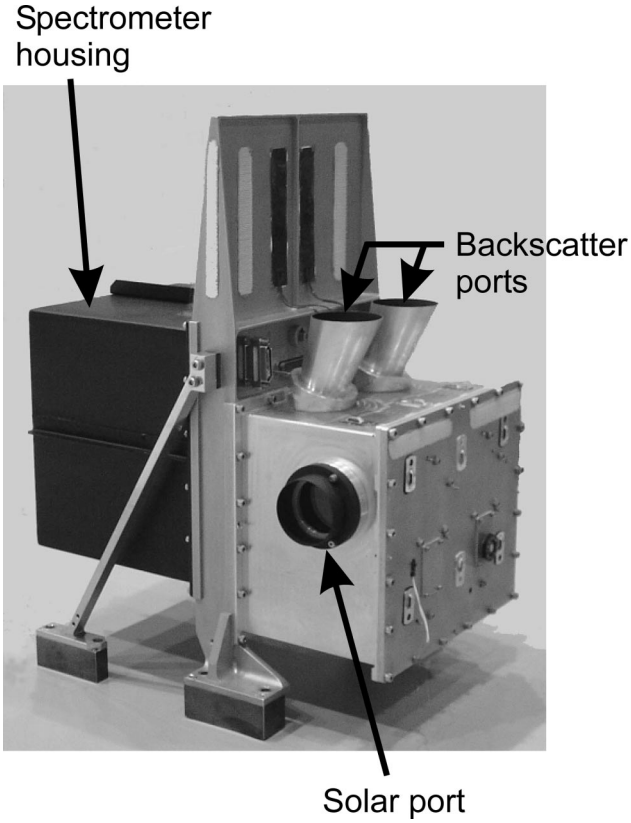

Fig. 1. Photograph of MAESTRO instrument, showing occultation and backscatter viewing ports.

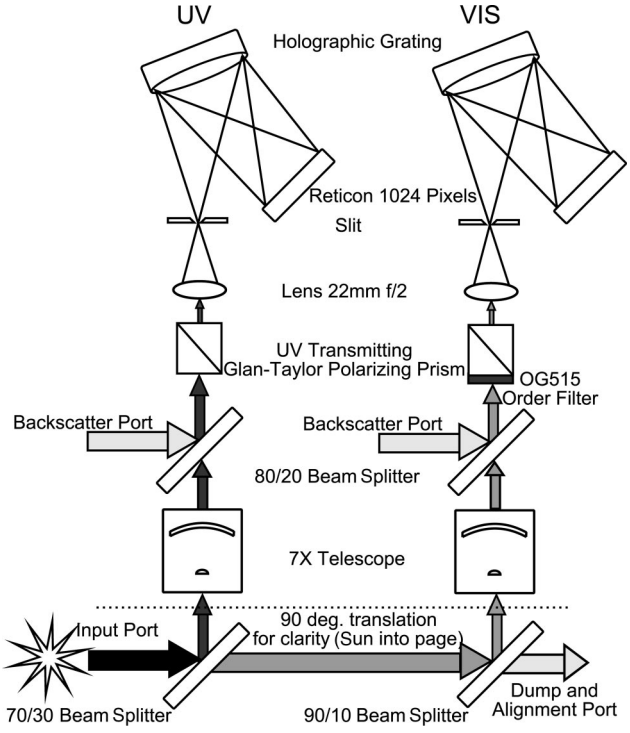

Fig. 2. Schematic of MAESTRO optics.

During an occultation, ~7% of the beam from the FTS primary pointing mirror is directed through a quartz window to the MAESTRO input optics using a pickoff mirror inside the FTS enclosure. The beam is then split between the two MAESTRO telescopes using two beam splitters situated just inside the solar input port. The first polka-dot beam splitter directs approximately two-thirds of the beam power to the UV spectrometer to help match the different signals in the UV and VIS regions, which result from the greater atmospheric scattering and absorption occurring in the UV spectral range. Most of the remaining light is passed to the VIS spectrometer by the second beam splitter and a small amount (~10%) of residual light is directed through an exit port, which was also used for alignment during prelaunch activities. Telescopes on each spectrometer provide an image magnification of 7×.

The FOV of each spectrometer is designed to include both the solar and the backscatter views by combining them with beam splitters. In solar occultation mode, the UV and VIS spectrometers use light from the suntracker entering through a common view port, but in backscatter mode, each spectrometer has its own input port. An 80/20 beam splitter situated at the entrance port of each spectrometer (after the solar telescope) allows the transmission of 80% of input radiation in backscattered view, but only 20% of the radiation if the instrument is observing the Sun. Each spectrometer, in spite of its small size, has an étendue ($A\Omega = 1.5 \times 10^{-5}\,\mathrm{cm}^2\,\mathrm{sr}$) similar to that of the Global Ozone Monitoring Experiment [10] (GOME) instrument by virtue of the spectrometer's large aperture and is therefore much more sensitive than needed for solar occultation observations; as a result, the loss of signal through the solar optics is of no consequence.

The entire satellite bus is pointed toward the Sun with modest pointing accuracy (~1°) using magnetic torque rods. An internal high-speed, two-axis suntracker pointing mirror, driven by a signal from a quadrant sensor operating at 1.55 μm, is used to direct the FTS FOV toward the radiometric center of the solar image. A pickoff mirror directs solar radiation from this suntracker to the MAESTRO spectrometers during occultation. Both the solar and backscatter ports are permanently open. To make backscatter measurements, the MAESTRO solar and backscatter FOVs are oriented 160° apart, with the backscatter FOV defined relative to the satellite coordinates at a fixed 20° off the antisolar vector, toward the nadir direction. When the instrument makes solar occultation observations at a tangent altitude of 100 km (essentially exoatmospheric), the backscatter FOV points into dark space. When the solar FOV is tangent at the satellite altitude (650 km), the backscatter FOV will point at the ground aft of the satellite at sunrise and ahead of the satellite at sunset at a point where the local solar zenith angle is approximately 80°. Once the local solar zenith angle at the satellite reaches 90°, the suntracker mirror is pointed off the Sun so that the solar input will be zero, and the backscatter signals will dominate the input.

After passing through the 80/20 beam splitter, each beam is fully linearly polarized by a Glan–Taylor polarizing prism. This prevents anomalous diffraction features of the diffraction gratings (Woods' anomalies [11]) from interacting with the scene intensity so that polarization will not influence the measurements during the backscatter mode. The angle between the polarizer and the spacecraft coordinates is fixed; therefore, the plane of polarization is always the same relative to the Sun–Earth-line-of-sight angle. The polarization for the backscatter port, determined as the direction of the electric vector, is perpendicular to the plane of the Earth, Sun, and satellite. The VIS beam also passes through an order-sorting filter, consisting of OG515 glass, to prevent light from higher orders of diffraction contributing to the measured signal. The UV spectrometer has no second-order diffraction problems thanks to the Planck falloff at short wavelengths for solar radiation.

The 50 μm $\times$ 2.5 mm entrance slits of the two spectrometers are projected to infinity by UV-corrected, 22 mm focal-length achromatic lenses. After passing through each slit, light is diffracted by a 5 cm $\times$ 5 cm, glass-substrate, 94 mm focal-length concave holographic diffraction grating, custom made by American Holographic Ltd.

The two independent MAESTRO spectrometers are fabricated on a common mechanical structure made of a 1 mm thick aluminum sheet. This spectrometer assembly contains the 22 mm lenses, slits, gratings, and detectors and is mounted inside the spectrometer housing denoted in Fig. 1. A single mount carries the diffraction gratings of both halves of the instrument. The grating mount is attached to the spectrometer structure by crossed-spring, wire flexure pivots and a torsion element. The angle of the gratings, the remaining degree of freedom of the grating mount, can be adjusted using a thermally scanned push rod to examine the sub-pixel-scale structure of the solar spectrum as observed by the instrument. The design of the grating mount includes temperature compensation of the focus of the spectrum so that changes in temperature do not cause changes in the instrument line-shape function (ILS). Figure 3 is a photograph of an early prototype of the MAESTRO spectrometer assembly, showing the kinematic sheet-metal structure that ensures a very stable and lightweight instrument.

The slit-lens-telescope combination of MAESTRO is designed to have a instrument FOV equivalent to roughly 1 km from SCISAT's 650 km orbit. A narrow vertical FOV is achieved by aligning a narrow 0.022° angular-extent axis of the entrance slit with the Earth radial direction using the orientation of the spacecraft. In the perpendicular (horizontal) direction, the slit's larger angular extent (0.65° on the UV and 0.89° on the VIS, as measured during preflight characterization) is designed to be centered on the Sun and larger than the Sun's width (~0.5°) to reduce the instrument's sensitivity to small horizontal satellite pointing motions (yaw), to capture as much signal as possible, and to permit averaging over intensity variations across the width of the Sun. This FOV also results in an instantaneous backscatter footprint of approximately 1.7 km $\times$ 70 km from SCISAT's 650 km orbit, although the long detector integration times used in backscatter measurements result in an effective footprint as large as 70 km $\times$ 70 km.

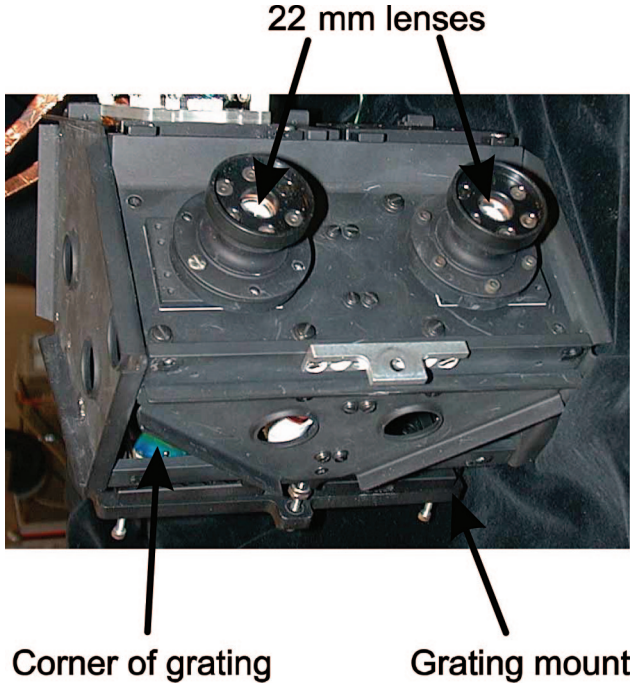

Fig. 3. Photograph of prototype MAESTRO spectrometer assembly. The corner of one grating is just visible in the lower left-hand corner of the diagram.

Two Reticon 1024-element, randomly addressable photodiode-array detectors, of the same type used in the GOME satellite instrument, detect the diffracted spectra. The detectors are intimately interconnected with a soft-programmable, XILINX field-programmable gate array-based (FPGA) microprocessor system, which selects the hardware readout algorithm and controls the timing of the observations made by the detector as well as coadding spectra and communicating with the instrument control computer. There is one computer system for each detector mounted on the readout electronics boards and one for the instrument control and communications functions. A fully synchronous state machine is embedded in the readout electronics FPGA as a peripheral of the 8 bit microcomputer. This state machine controls the observation process and orchestrates the collection and coadding of spectra during a period when the microcomputer is actually turned off to avoid the generation of asynchronous noise.

Occultation measurements span a very large dynamic range, both as a function of tangent altitude and as a function of wavelength; observation tangent heights range from the surface to 100 km over an atmosphere whose density changes exponentially with

altitude, while the strong Hartley–Huggins ozone absorption bands (<350 nm), in combination with the Rayleigh scattering that increases as λ^{-4}, remove most radiation in the UV. This large dynamic range presents a challenge in terms of the design of the MAESTRO detection electronics if optimal measurements are to be made. To address this issue, the MAESTRO detector electronics have been designed to operate in various measurement modes through the use of a randomly addressable detector, where particular pixels of the detector can be integrated and read out independently from other pixels in the array.

The design of the Reticon photodiode array permits its use in various ways. Internal transmission gates allow individual pixels to be either isolated from a common video line or connected to it. This selection can be done in one of two ways: individual gates can be turned on using an internal decoder that allows a 10 bit address word to select a particular pixel to be read and reset, or a separate input can be used to connect all pixels simultaneously to the video line, causing all pixels to be simultaneously reset to an external reference potential of 2.5 V. In both modes, the current to reset the detector elements is supplied by an electrometer amplifier tied to a precision voltage reference. The measurement of light flux is performed by determining the amount of charge lost because of exposure to light when the pixels are reset. A high-resistance feedback resistor (300 kΩ) in the electrometer circuit produces a measurable signal, which is amplified and then digitized by a radiation-hardened, 16 bit analog-to-digital (A/D) converter.

MAESTRO measurements use two main detector readout modes. The first mode, the multiple reset mode, can be used for very bright observations. At very high signal levels, the short integration times (10–150 μs) are comparable with the time for an individual pixel readout (~14 μs), so that it may be that only one pixel can be read between simultaneous resets of the array pixels before other pixels saturate. This type of observation begins with the starting pixel address placed on the array address bus and the array held in the reset state. In this state, the electrometer resistor is shorted by a transmission gate, and the pixels are all continuously recharged via the reset circuitry. The pixel is read by removing the reset, waiting for a short integration time (e.g., 10–150 μs), and then asserting the address strobe to read out the selected pixel. The process of reset, integrate, and read is repeated for each pixel separately until the entire array has been interrogated.

The second mode is the parallel integration mode. For low light levels and long detector integration times, all pixels on the array are integrated simultaneously, and then each pixel is read out in sequence, with no pixel resets between reads. The observation begins with the array reset control line holding all diodes in reset state, and after a predefined integration time, the address strobe is asserted. This gates the first, addressed pixel onto the video line where the reset charge is measured and digitized. Subsequently, the address strobe is held unchanged, and each of the photodiodes is read out, in turn, by changing the pixel address applied to the array followed by A/D reads. Changing the address automatically isolates the already reset, selected photodiode pixel and charge, which then begins integrating for the next scan. The majority of MAESTRO measurements in occultation are made with midrange integration times, which require a variation of the parallel integration mode readout system. In this mode, the array is divided into a number of equal-sized readout groups consisting of 8–512 pixels. After being reset, the entire array is integrated, all pixels within a group are read out, and then the entire array is again reset and integrated, and the next group of pixels read out until the full spectrum is assembled.

The array is always read from the long-wavelength to the short-wavelength end of the detector to ensure that the pixels with the highest light levels (when the Sun is attenuated by the atmosphere) have the shorter total integration times. Each spectral measurement uses the same base integration time for every pixel on the array (determined from the expected signal at each tangent height), but the time required for signal readout of each pixel means a pixel continues to integrate while waiting for other pixels to be read. Therefore, the effective integration time of a pixel is always longer than the base integration time and depends on its position on the array relative to the first pixel in the readout queue.

Each occultation observation is based around a measurement cycle of 330 ms, chosen so that it is possible for measurements to be made at 1 km altitude intervals in the case where the beta angle (the angle between the satellite orbital plane and the Earth–Sun vector) is zero. Each spectral measurement consists of a preread measurement in the multiple reset mode with a fixed integration time for all altitudes and another measurement optimized by mode and integration time for the expected light level at the particular tangent altitude. These optimized measurements usually consist of two to three individual spectra that are coadded to maximize the signal-to-noise ratio within the 330 ms measurement time. The number of pixels in a group and the integration time are chosen according to the expected signal level at a given tangent height based on a radiative transfer model of the atmosphere. Command tables defining the readout parameters are uploaded to the satellite and stored in the instrument memory. They are produced for different beta angles to match the observation timing to the timing of the occultation. Figure 4 describes a sample series of measurement parameters used for a single occultation. Based on the expected solar occultation signal at every tangent height, each observation is assigned (1) a pixel integration time, (2) the number of pixels to integrate in a group before resetting the detector to prevent saturation during detector readout for that integration time, (3) the resulting number of readout groups of pixels across the 1024-pixel array, and (4)

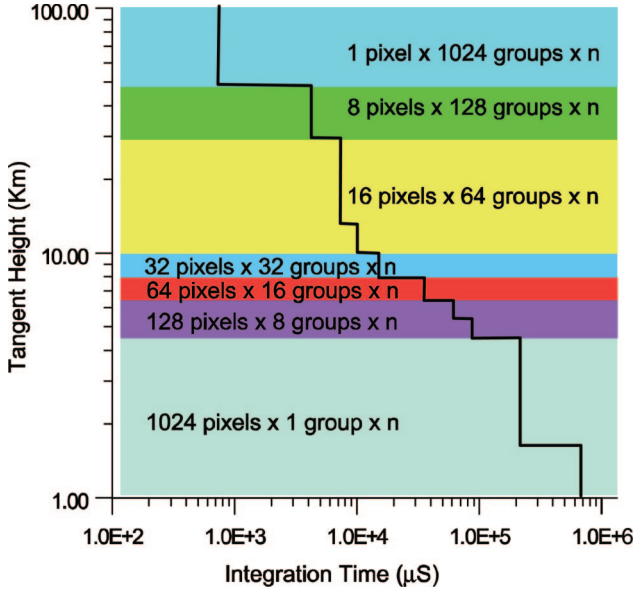

Fig. 4. Schematic of sample detector measurement parameters (number of pixels read in a group before detector reset × number of resulting pixel groups across detector × number of coadded spectra n), and pixel integration times as a function of tangent height for one occultation sequence.

the number of coadded spectra, n, required to complete a measurement cycle of roughly 330 ms. The selection of the number of pixels in a group is dependent on the integration time, and the same group count (but different n) may sometimes apply to slightly different integration times, as evidenced by the step features in the integration time in the (16 pixels × 64 groups × n), (128 pixels × 8 groups × n), and (1024 pixels × 1 groups × n) bands.

B. Preflight and On-Orbit Characterization

The MAESTRO and FTS instruments were characterized together at the Instrument Characterization Facility at the University of Toronto during February and March 2003. The goal of the characterization tests was to assess the performance of the instruments in a simulated orbital environment. To achieve this aim, the instruments were mounted on a replica of the satellite baseplate and placed in a vacuum chamber for the duration of the characterization period. A cylindrical liquid-nitrogen-cooled shroud was positioned around the instruments to simulate the thermal environment of space, and a liquid-helium target positioned adjacent to the FTS detector radiator cone was used to simulate the FTS's deep-space radiator view. Fluid at various temperatures was pumped through a coiled pipe in thermal contact with the bottom of the baseplate to simulate the thermal fluctuations encountered on orbit due to periodic changes in thermal loading from the Earth and Sun. A suite of characterization tests was repeated for different baseplate temperatures ranging from −25° to 25 °C.

Light from various sources was directed through a window into the vacuum tank to the FTS pointing mirror and, in turn, a portion of this light was passed on to MAESTRO as in an occultation measurement. A solar simulator source was built to simulate an occultation measurement for both instruments by combining IR light from a high-temperature (3000 K) blackbody source with VIS light from a 1000 W quartz-halogen lamp using a germanium beam combiner. By comparing MAESTRO laboratory spectra with solar spectra taken on orbit, the irradiance produced at the instrument by the quartz-halogen lamp was determined to be roughly $\frac{1}{100}$ of that of the Sun. The combined beam was directed through a gas cell and focused on a field stop with a circular aperture equivalent to the angular extent of the Sun. A slowly moving knife-edge shutter was placed next to the field stop to simulate the effect of the solar disk changing shape during satellite sunrises and sunsets. The system was used to perform several instrument characterization tests, and also to make ozone and NO_2 gas cell measurements simultaneously with the FTS [12,13]. Dufour *et al.* [12] describe the design of the optical system in detail, as applied to the ozone gas cell tests. In addition to tests performed with the main optical test system and solar simulator, several bench tests were performed on MAESTRO using lasers and emission lamps to examine instrument line shape and wavelength-pixel dispersion.

In combination with preflight calibration, on-orbit tests and data analysis allow full and updated instrument characterization. The following sections summarize the characterization of the instrument from the combination of preflight and on-orbit tests.

1. *Instrument Line Shape*

Diode lasers at wavelengths of 532, 670, and 830 nm, as well as a mercury emission lamp, were used preflight to examine the instrument line shape. The FWHM of the line shape is used as a measure of the instrument's spectral resolution. The FWHM changes somewhat across both detectors but was found to be approximately 1.5 nm in the UV, and between 1.9 nm and 2.2 nm in the VIS instrument. Figure 5 shows the VIS instrument line-shape function determined from a laser measurement at 830 nm, as well as additional line shapes determined at nearby wavelengths on-orbit. The on-orbit VIS line shapes were determined by deconvolution from observed on-orbit spectra and modeled high-spectral-resolution absorption spectra. The high-resolution absorption of molecular oxygen was modeled for a set of observations in the O_2 *A* band (at 762 nm) and the *B* band (at 690 nm) using a line-by-line radiative transfer model with O_2 line parameters from HITRAN 2004 [14] and the ACE *a priori* temperature profiles described in Boone *et al.* [7], which at altitudes below 30 km are derived from the operational analyses of the Global Environmental Multiscale model of the Canadian Meteorological Centre. These theoretical high-resolution spectra were used to deconvolve an average line shape from observed MAESTRO spectra. The *A*- and *B*-band-determined line shapes are similar in shape to each other and differ mainly in their FWHMs, which is to be

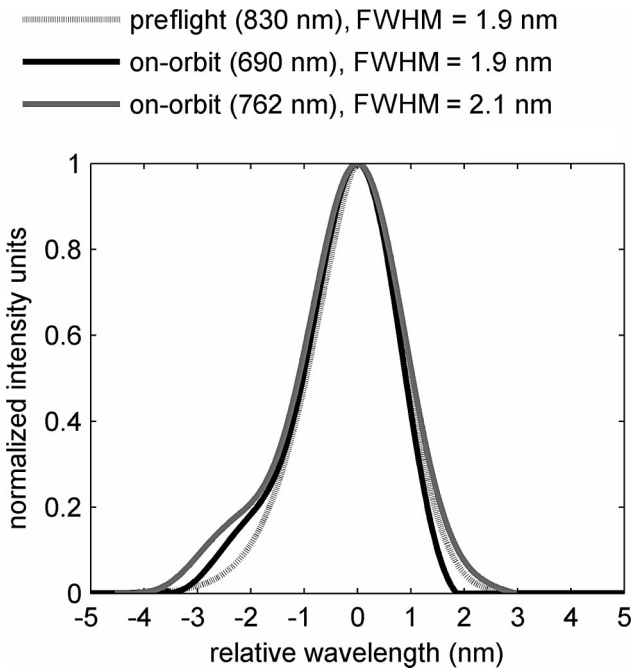

Fig. 5. Instrument line shape for the VIS spectrometer, showing the ILS measured preflight with an 830 nm diode laser, as well as two ILS functions determined by deconvolution of the ILS from occultation measurements in the O_2 *A* and *B* bands.

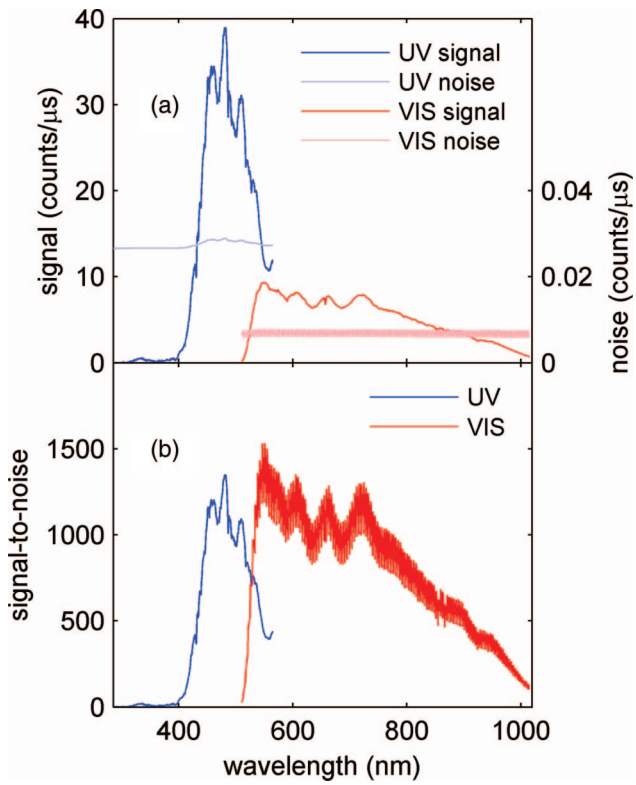

Fig. 6. (a) Signal and noise levels for a sample high-Sun measurement collected at the beginning of sunset occultation ss4043 (13 May 2004 09:48:56UT at 65.3 °N, 75.2 °E). Both the signal and noise have been corrected for effective integration times and are shown in detector counts per microsecond. (b) The measurement's resulting signal-to-noise ratio. The curves representing noise and signal to noise on the VIS spectrometer show structure in eight pixel groups resulting from the use of the Parallel Integration readout mode using 8 pixels per readout group.

expected as the spectral resolution changes across the detector. They suggest that the on-orbit instrument line shape is more asymmetric than the one originally measured in the laboratory. The difference in the asymmetry of the line shape between the prelaunch tests and the on-orbit retrievals is most likely due to changes in the intensity distribution of light across the instrument aperture. While a good effort was made to uniformly fill the FOV during ground tests, there may have been a difference between the distribution of light in the tests as compared with the filling of the FOV on orbit.

2. *Signal-to-Noise Ratio*

The analysis of high-Sun spectra indicates that both the UV and VIS spectrometer pixels have an average of ~4.1 A/D counts of readout noise (1σ). This is an improvement over the approximately seven counts of readout noise measured in the laboratory during characterization. At maximum levels, the signal provides an additional random (shot) noise component of nearly four counts. While the 16 bit A/D converter allows 65,536 counts on the detector, in practice a full well readout from the detector is designed to be approximately half-scale. At half-scale on the detector, the signal-to-noise ratio can be as high as 3000. However, observations are generally limited to ~10,000 counts to avoid any risk of saturation or possible nonlinearities at higher count levels, and most high-Sun measurements are designed to operate at peak signal-to-noise ratios of approximately 1500.

Figure 6(a) shows the signal and estimated noise as a function of wavelength and corresponding pixel number for a typical high-Sun measurement collected during sunset occultation ss4043 (13 May 2004 09:48:56UT at 65.3 °N, 75.2 °E, referenced to the 30 km subtangent location). The signals in the figure are shown in detector counts per microsecond after correction for each pixel's effective integration time. Their corresponding noise values are shown in the same units. These spectra are uncorrected for absolute response, and therefore, the relative magnitudes of the UV and VIS signals are not expected to appear consistent. The noise is a function of readout noise, shot noise (and therefore total signal), and the number of coadded spectra (in this particular case, the UV signal results from only one spectrum, but the VIS is a product of onboard coadding of three spectra). Figure 6(b) shows the resulting signal-to-noise ratio of this high-Sun measurement. The VIS spectrometer has been read out in the 8 pixel per group parallel integration mode; the individual pixel readout times (~14 μs) are comparable with the individual base pixel integration times (308 μs), and therefore the last pixel read in a group experiences a noticeably longer effective integration time than the first pixel as it waits for readout. This difference in signal across a group of eight pixels is quite apparent in the

noise and signal-to-noise spectra, which cycle in amplitude every eight pixels (however, not in the signal spectra, which have been corrected for this effect). The UV spectrum was collected in the multiple reset mode where each pixel is integrated separately, and then the entire array is reset after each read, so that all effective pixel integration times are the same, and its noise and signal-to-noise do not show features from pixel grouping.

3. Absolute Response

The absolute response of the spectrometer was measured in the laboratory using a Spectralon Lambertian diffuser plate illuminated by the quartz-halogen lamp. The solar UV spectra showed a maximum absolute response of 1.3×10^9 (counts/s)/(W m^{-2} nm^{-1}), while the peak sensitivity of the VIS spectra was 6.5×10^8 (counts/s)/(W m^{-2} nm^{-1}). Knowledge of the absolute sensitivity is not strictly necessary for occultation measurements, which require only the solar reference spectrum measured at high Sun, but it allows a proper comparison of instrument response before and after launch with comparisons of high-Sun measurements on orbit. As can be observed in Fig. 6, on orbit, all solar radiation at wavelengths less than 400 nm is virtually extinguished from the solar spectra. This was not observed in quartz-halogen lamp spectra collected on the ground where the responsivity across the UV detector was strong for all wavelengths. The cause of this reduction in intensity cannot be decisively determined with the instrument in orbit. Only the occultation spectra are affected; the backscatter spectra contain the short wavelength signals below 400 nm. As a result, molecules absorbing at wavelengths less than 400 nm are unfortunately not observable in occultation, including BrO, OClO, and SO_2, and the Hartley–Huggins bands of O_3. Fortunately, the primary data products of O_3 (measured in the Chappuis band by the VIS spectrometer, and the short-wavelength edge of the Chappuis band by the UV spectrometer), NO_2, and aerosols, as well as H_2O and O_2, are not affected.

4. Field of View

During preflight characterization, FOV maps of the spectrometer slits were obtained by deflecting the beam of an incoming laser with wavelength 532 nm to a variety of angles using the suntracker mirror and measuring the resulting signal intensities on both spectrometers. The FOV coincidence of the two slits was confirmed, and it was determined that the long axes of the slits were parallel with each other to 0.4°. The elevation extent of both slits was determined to be 0.022°, defined by the FWHM of the response. The azimuthal extents were measured at 0.65° (UV) and 0.89° (VIS). The FWHM slit size results in an instrument FOV of 1.2 km in the vertical and approximately 35 (UV) and 45 (VIS) km in the horizontal for a 22 km tangent altitude. During an occultation the signal comes only from the solar disk and the signal extent in the horizontal is then ~25 km. After launch, scans across the solar disk using the suntracker mirror corroborated the FOV knowledge on orbit.

4. Measurements

SCISAT was launched under a cooperative launch agreement with NASA on 12 August 2003 by a Pegasus Launch Vehicle released from a Lockheed 1011 aircraft off the coast of California, near Vandenberg Air Force Base. As soon as the satellite was in orbit, the FTS and MAESTRO were turned on. An extensive engineering commissioning phase ensued, leading up to full instrument operations in February 2004. Engineering tests, beginning in October 2003, involved collecting test spectra to determine instrument health. These included occultation observations, exercising the thermal scan rod, measuring the internal photodiode test light sources, and a trial backscatter observation. MAESTRO began regular operations on 21 February 2004. As of mid-January 2007, MAESTRO had collected 7175 sunrise, 8110 sunset, and 1787 backscatter observations.

An occultation sunrise or sunset measurement sequence typically takes 1–3 min, depending on the angle of the Sun relative to the orbital plane, and consists of approximately 60 spectra collected at tangent altitudes between 0 and 100 km (however, most useful measurements do not extend below 5–10 km due to the presence of clouds) and 20 spectra collected between 100 and 150 km for calculation of a high-Sun reference spectrum. A series of 80 spectra are also collected using identical detector commands, either immediately before (sunrise) or after (sunset) the occultation when the Sun is below the horizon, to use in the calculation of detector dark current. Measurements from the beginning of the mission to August 2005 tend to be densely spaced in the vertical at tangent altitudes below ~50 km, with a spacing between spectra of ~300 m to 2 km, while spectra were collected only every 5 km above a 50 km tangent. The measurement command tables were modified on 10 August 2005 to allow a 2 km vertical spacing between measurements at altitudes above 50 km. Occultations collected after this date contain between 60 and 80 spectra collected at tangent heights below 100 km.

Backscatter measurements are a secondary measurement mode and are only collected as opportunity presents. The availability of satellite command and control resources primarily determines the frequency of backscatter measurements. Each backscatter measurement command results in the collection of 160 spectra in sequence, cycling between three different integration times to ensure spectra are neither saturated nor too weak with changing albedo below the satellite.

5. Data Processing: Version 1.2 Retrieval Algorithm

The MAESTRO retrieval algorithm is still under development. Here we present the algorithm for the version 1.2 release of MAESTRO data. The processing of MAESTRO occultation data involves two major steps. The first is the conversion of raw data (Level 0) to spectra calibrated in wavelength and corrected for

various instrument parameters, such as pixel integration times and dark current, as well as instrument stray light (Level 1), and the second is the conversion of calibrated spectra to extinction, slant column densities, and vertical profiles (Level 2). In this section, the data processing is described with reference to the primary occultation measurement mode. Although the initial Level 0 to Level 1 processing and spectral fitting methods also apply to backscatter measurements, backscatter measurements are a secondary measurement goal and have not yet been examined extensively, and no results will be presented in this paper. Version 1.2 MAESTRO data provide ozone and NO_2 profiles, as well as total wavelength-dependent atmospheric optical depth extinction. The analysis of ozone and NO_2 are presented here. The development of the aerosol product is still ongoing and results are not discussed in detail in this paper.

A. Level 0 to Level 1 Processing: Calibration

The data from the SCISAT spacecraft are downlinked to several ground stations, assembled at the Canadian Space Agency (CSA) Mission Operations Centre in St. Hubert, and transferred to the Science Operations Centre (SOC) computers at the University of Waterloo, where the mission archive resides. MAESTRO data are also archived separately at the University of Toronto and Environment Canada in Toronto, Ontario. The Level 0 MAESTRO data are archived as binary files, and contain science data from the instrument as well as instrument engineering data collected from the main SOC database. Geolocation data are also provided by the SOC.

The conversion of raw spectra to calibrated spectra has two major steps: correcting raw spectra and assigning wavelengths to the spectra. The signal analyzed in an occultation measurement is the wavelength-dependent transmission of the atmosphere, which is defined by the ratio of the intensity of the spectrum collected during the occultation, when the atmosphere is absorbing and scattering, to a high-Sun reference spectrum, which can be collected at any point in the orbit when the satellite–Sun vector does not intersect the atmosphere. In practice the high-Sun spectra are taken as close in time to the atmospheric spectra as possible. As long as the instrument can measure a reliable high-Sun reference spectrum from orbit, the data do not require absolute calibration using the instrument responsivity. However, the Level 0 to Level 1 processing must apply a number of corrections to the raw data to remove the effects of the variable pixel integration times across the detector array and the different readout modes between spectra, and to correct for instrumental stray light, electronic fixed-pattern offset, dark current, and charge carryover caused by resetting the detector very quickly.

The on-orbit wavelength calibration uses Fraunhofer solar absorption features to determine the relationship between each pixel and its corresponding wavelength. The pixel-wavelength calibration fits the wavelengths of an observed MAESTRO high-Sun reference spectrum from each occultation to those from the higher spectral resolution (0.5 nm) ATLAS-1 composite solar reference spectrum of Thuillier *et al.* [15], degraded to the MAESTRO resolution by convolution with the MAESTRO instrument line-shape function. While the ATLAS-1 solar reference spectrum is calibrated in absolute intensity, the observed MAESTRO solar spectrum is not. In addition, the observed spectrum is contaminated with a cyclic change in sensitivity because of etaloning on the detector. To properly align the spectral features, a high-pass filter is applied to each spectrum so that only the high-frequency spectral information remains. These high-frequency spectra are then normalized to each other in intensity for the purpose of the wavelength-calibration procedure.

An iterative, least-squares minimization is used to fit the wavelengths of the observed high-pass-filtered spectrum to the ATLAS-1 spectrum by determining coefficients for a polynomial that describes the wavelengths as a function of pixel number on the array. It was determined empirically that the use of a seventh-order polynomial provides an acceptable match over the spectral fitting window.

Figure 7 shows all MAESTRO occultation spectra in detector counts per microsecond for occultation number ss4043, after the detector and wavelength calibrations described above have been applied. For clarity, all the VIS spectra have been scaled by one constant factor to match the UV at the long-wavelength end of the UV spectrum. The most intense spectrum is a solar reference spectrum collected just before sunset, at a tangent height of approximately 150 km. As these spectra are not calibrated in absolute intensity, the instrument responsivity is still visible in the falloff of intensity at short wavelengths in the VIS spectra (caused by the OG515 order filter), and there is visible

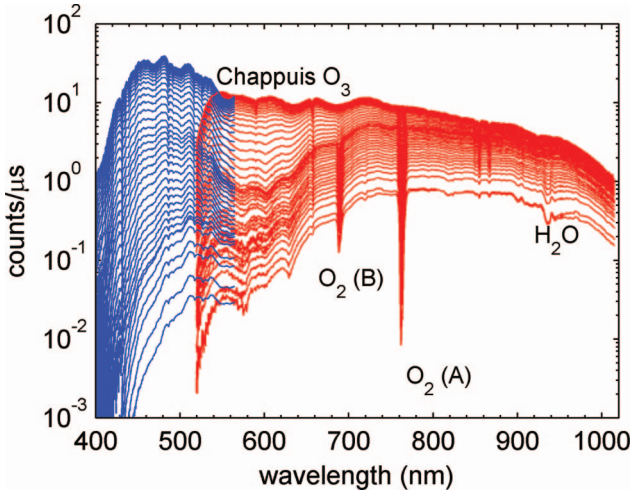

Fig. 7. MAESTRO UV (blue) and VIS (red) spectra in detector counts per microsecond from occultation ss4043, after scaling for detector integration time, fixed-pattern offset, dark count, and grating stray light. The VIS spectra are scaled by a constant factor to align with the intensity of the UV spectra at the UV's long-wavelength end.

evidence of detector etaloning in the oscillatory changes in sensitivity as a function of wavelength (e.g., the broad peak features between 450 and 550 nm in the UV and 600 and 750 nm in the VIS spectra). Several prominent atmospheric absorption features are immediately visible in these calibrated spectra, including the O_3 Chappuis absorption band near 600 nm, water vapor near 950 nm, and the O_2 *A* and *B* bands near 762 and 690 nm, respectively.

B. Level 1 to Level 2 Processing: Optical Depths, Slant Column Densities, and Vertical Profiles

To derive constituent amounts from the Level 1 spectra, a nonlinear, least-squares spectral fitting code is used to fit forward-modeled effective optical depths (at MAESTRO resolution) to those apparent optical depths observed during the occultation. The optical depth spectra are calculated by

$$\tau(\lambda_p) = -\ln\left[\frac{I(\lambda_p)}{I_0(\lambda_p)}\right], \tag{1}$$

where $\tau(\lambda_p)$ is the optical depth at each pixel with wavelength λ_p, $I(\lambda_p)$ is the occultation spectrum, and $I_0(\lambda_p)$ is the reference spectrum at high Sun for wavelength λ_p. As long as the instrument responsivity remains constant between the time the solar reference spectrum, I_0, is taken and the occultation spectrum, I, is measured, the instrument responsivity function is removed in the calculation of optical depth, and therefore its knowledge is not required. Figure 8 shows optical depth spectra for several sample tangent heights derived from the ss4043 occultation and high-Sun spectra shown in Fig. 7.

The v1.2 optical depth calculation assumes that MAESTRO views the same part of the Sun during exoatmospheric and occultation measurements and that inhomogenieties across the Sun's surface may be ignored. MAESTRO observations use light integrated across the full width of the solar disk to minimize the impact of spatial variations of intensity across the Sun's surface. The suntracker is designed to reference the center of the Sun, and on-orbit tests confirm its performance. There will be some variation in the FOV location on the Sun due to the effective movement of the FOV in the Earth's radial direction, especially at lower tangent heights (<20 km), as refraction and attenuation distort the solar image and shift the pointing direction upward. These effects are under study using scans done across the solar disk when collecting exoatmospheric spectra. Appropriate corrections to future versions of the retrieval algorithm will be made if required. Data comparisons done to date suggest that these effects are not likely to be large [16].

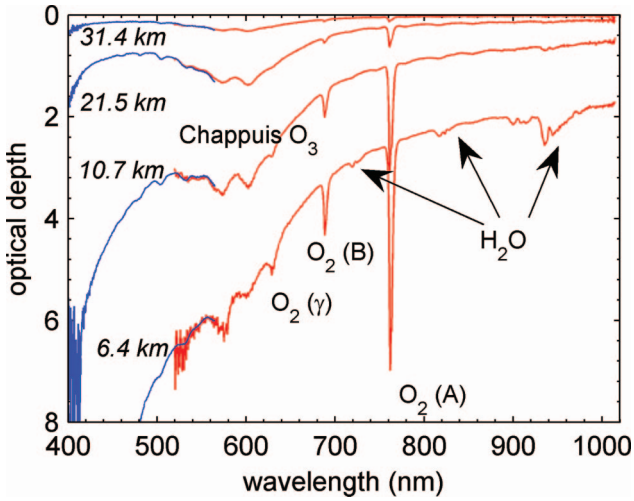

Fig. 8. MAESTRO UV (blue) and VIS (red) optical depth spectra for four sample tangent altitudes from occultation ss4043.

A global-fitting algorithm, similar to that described by Carlotti [17] for IR limb sounding, has been developed for the MAESTRO analysis, but has not yet been implemented operationally. A global-fitting code allows the retrieval of constituent profiles from a simultaneous fit of all MAESTRO spectra during an occultation. The current data release (version 1.2) uses a classic two-step method to derive vertical volume mixing ratio profiles. Spectral fitting is used to derive a slant column density (SCD) for each spectrum, and these slant column densities are subsequently used to calculate a profile. The retrieval process does not make use of any *a priori* information or other auxiliary constraints such as smoothing. The spectral-fitting code was originally developed for fitting spectra from MAESTRO's precursor instrument, the CPFM, used on the ER-2 aircraft [8], and retrieves the apparent SCD of a trace gas for each individual spectrum along the line of sight of that observation. For radiation traveling along a path of length L, the optical depth is defined by

$$\tau(\lambda) = \int_0^L \sigma(\lambda,\ l)n(l)\mathrm{d}l, \tag{2}$$

where $\sigma(\lambda, l)$ is the cross section representing the absorption features of a particular absorber and may be dependent on local pressure or temperature along the path, and $n(l)$ is the number density of the constituent in segment dl of the path. The SCD, X, represents the total amount of the constituent along the line of sight of the observation (units of molecules per area), $\int_0^L n(l)\mathrm{d}l$. In terms of SCD, the total monochromatic apparent optical depth (the sum of optical depths of all individual constituents) is written as

$$\tau = \tau_{O_3} + \tau_{NO_2} + \cdots + \tau_{\text{Rayleigh}} + \tau_{\text{aerosols}},$$

$$\tau = \sigma_{O_3}X_{O_3} + \sigma_{NO_2}X_{NO_2} + \cdots + \sigma_{\text{Rayleigh}}X_{\text{Rayleigh}} + (\sigma_c X_c + \sigma_l X_l + \sigma_s X_s)_{\text{aerosols}}. \tag{3}$$

In addition to retrieving trace-gas amounts, each spectral retrieval also determines the magnitudes of individual constant (X_c), linear (X_l), and quadratic (X_s) SCD offsets that are used to account for background aerosol absorption by using effective cross

sections for σ to represent the wavelength dependency of the offsets. Wavelength shift and stretch terms are also fit to fine-tune the pixel-wavelength assignments to within 0.01 nm. Rayleigh scattering is accounted for by retrieving an air column density using a Rayleigh scattering cross-section vector.

The various main terms fit and modeled in each spectrum are described in Table 1 as main sources of extinction. The spectral fits are performed across a wide range of wavelengths, from 420 to 545 nm in the UV and 530 to 755 nm in the VIS, and are modeled at a wavelength spacing of 0.1 nm. O_3 and NO_2 are fit using cross sections from the GOME flight model [18,19], collected at 202 and 221 K, respectively. Both O_3 and NO_2 cross sections have some temperature dependency. The use of the largely temperature-independent Chappuis band for O_3 retrievals means that the uncertainty associated with the use of cross sections collected at different temperatures is minimal (<1%). The temperature dependency of NO_2 is larger, and the uncertainty associated with using a cross section at a fixed temperature is estimated to be between 5% and 10%. All trace gases and spectral parameters are fit using a direct spectral fit, with the exception of NO_2, which is fit using a differential optical absorption spectroscopy method. The NO_2 cross section is divided into high- and low-frequency components using a smoothing filter, and the high-frequency component of the cross section is fit independently to determine the retrieved NO_2 SCD. An amount of absorption from the smoothed cross section is also included, based on the same SCD of NO_2. Although not currently operational data products, H_2O, O_2, and O_2–O_2 are also forward modeled and fit in the retrieval to account for their spectral contributions. O_2–O_2 column density is determined using cross sections from Greenblatt *et al.* [20]. Currently the spectra are corrected for H_2O and O_2 *B* and γ band absorption by retrieving approximate SCDs using a moderate-resolution effective cross section determined from a line-by-line radiative transfer calculation through one representative 20 km tangent path using line parameters from HITRAN 2004 [14].

The SCDs of O_3 and NO_2 retrieved for occultation ss4043 are shown in Fig. 9 as a function of time elapsed since the beginning of the occultation observation sequence and as a function of corresponding tangent altitude below 100 km. These figures show the SCDs derived for NO_2 from the UV channel, and ozone from the UV and VIS channels. For comparison, the FTS SCDs are also plotted for ozone and NO_2. (The FTS data processing does not retrieve SCDs but rather inverts spectra directly to profiles. Therefore, the FTS SCDs plotted in Fig. 9 are not v2.2 products from the FTS but are from integration along the MAESTRO line of sight using the FTS's ozone and NO_2 profiles.)

Due to the nature of ozone absorption in the UV and VIS spectrometer wavelength regions, the stratospheric VIS retrieval of ozone is generally considerably more accurate than that only performed from the UV spectrometer, using spectra between 420 and

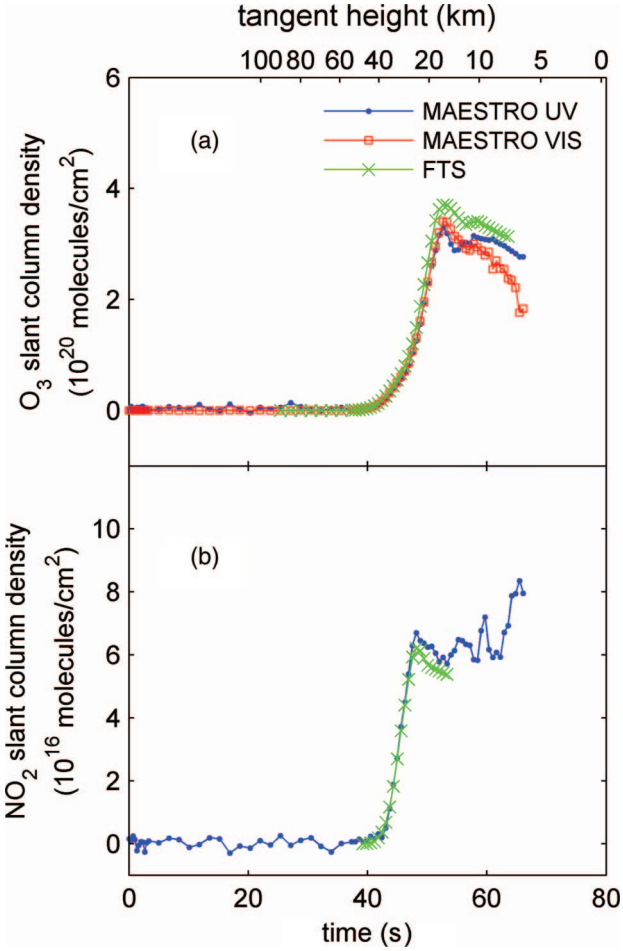

Fig. 9. Slant column densities for occultation ss4043 of (a) ozone derived from the UV and VIS spectrometers and FTS profiles and (b) NO_2 derived from the UV spectrometer and FTS profiles. The slant column densities are plotted as a function of time elapsed since the beginning of the occultation sequence, as well as their corresponding tangent heights. See the text for a discussion of uncertainties.

545 nm. The retrieval of ozone in these spectral regions uses only the short-wavelength edge of the Chappuis band, where there are other strong broadband spectral features from aerosols and Rayleigh scattering whose retrieval may interfere with that of ozone. In the troposphere and lower stratosphere, where the peak of Chappuis ozone removes a considerable amount of light in the short-wavelength end of the VIS detector and Rayleigh scattering is intense, the VIS integration times must still remain relatively short to ensure that the detector does not saturate at its longer wavelengths. In this case, ozone retrieved using the UV spectrometer is comparable in reliability with the retrieval from the VIS spectrometer (see, for example, the relatively large noise in optical depth spectra collected at 6.4 and 10.7 km in Fig. 8 in the peak of the Chappuis band).

Vertical profiles of trace gases are derived from MAESTRO using a nonlinear Chahine relaxation inversion [21]. Figure 10 shows sample ozone and NO_2 profiles for three occultations, including ss4043,

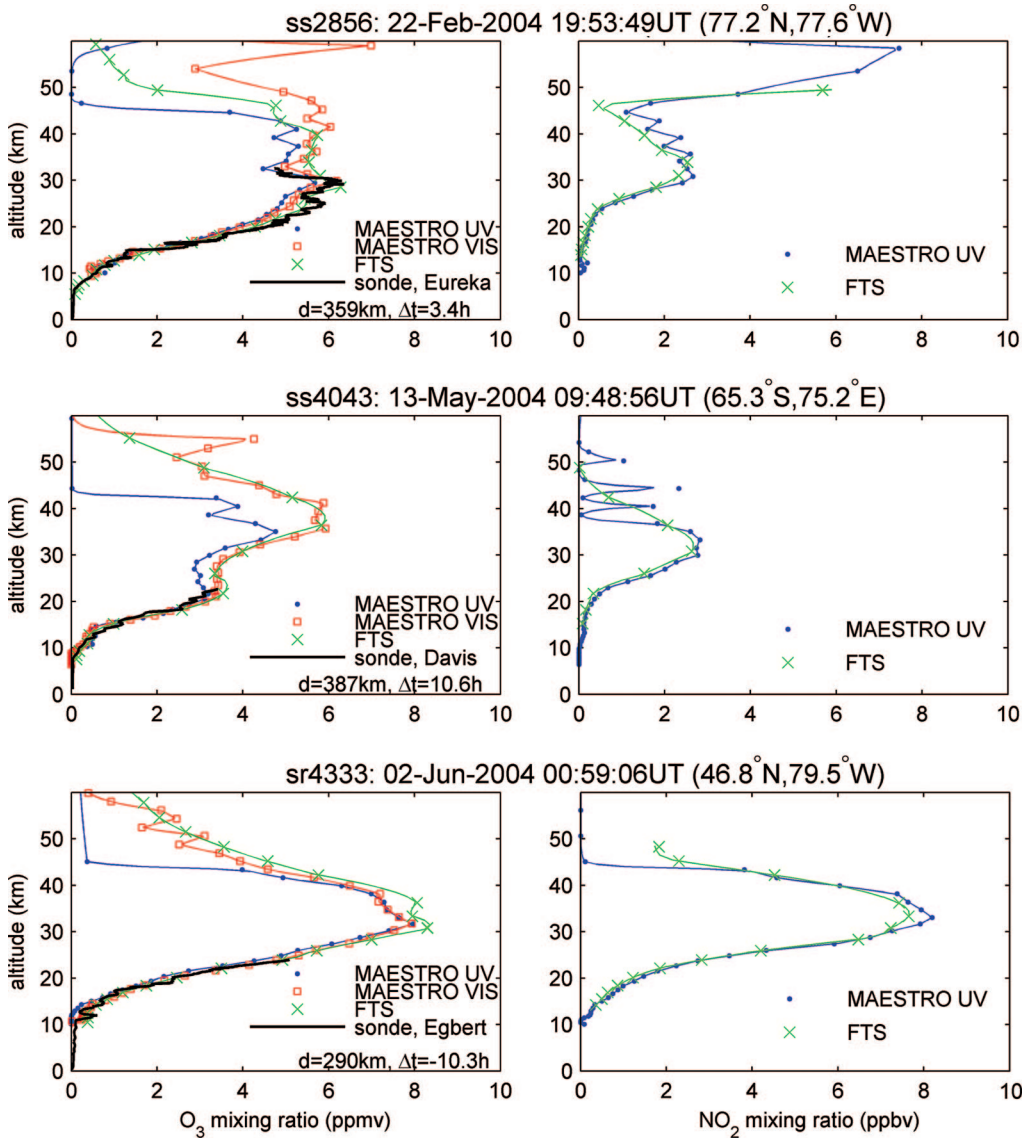

Fig. 10. Volume mixing ratio profiles of ozone (in parts per 10^6 by volume) and NO_2 (in parts per 10^9 by volume) retrieved from MAESTRO and the FTS for sunset occultations ss2856 (Arctic winter) and ss4043 (Antarctic fall/winter), and sunrise occultation sr4333 (midlatitude summer), as well as ozone mixing ratios from coincident ozonesonde flights. The site of the ozonesonde launch is noted in each legend, as well as its distance d from the 30 km subtangent point of the ACE occultation and the time in hours elapsed since the occultation, Δt. The data points signify the retrieved amount at each tangent point, while the solid curves represent the profiles interpolated onto grids equally spaced in altitude (every 1 km for the FTS and 0.5 km for MAESTRO). See the text for a discussion of uncertainties.

which was derived from the SCDs pictured in Fig. 9. Figure 10 also shows the FTS v2.2 ozone and NO_2 profiles derived at the University of Waterloo Science Operations Centre for the same occultations, as well as ozone profiles from ozonesonde launches that coincided with ACE observations. The latitude–longitude location of each occultation is referenced to its 30 km subtangent point. The data points in the profiles denote the retrieved volume mixing ratios retrieved at the tangent heights from either the MAESTRO or FTS occultation. The solid curves represent the profiles interpolated onto equally spaced grids. The spacing of these altitude grids is 0.5 km for MAESTRO and 1 km for the FTS. Both the tangent and interpolated profiles are available in the MAESTRO v1.2 and FTS v2.2 data releases.

A full validation of the preliminary v1.2 MAESTRO ozone and NO_2 products has been performed by Kar *et al.* [16], including comparisons with the FTS and coincident profiles from ozonesondes, SAGE III, and POAM III. As a result, a detailed assessment of retrieval performance with respect to the FTS and other instruments is not presented here. We can, however, give typical estimates of retrieval uncertainties for individual profiles. Table 2 lists precision estimates from retrieval noise at different altitudes for a typical Arctic spring retrieval of VIS ozone and UV NO_2 profiles and for the slant columns tangent at

Table 2. Estimated Errors in O_3 and NO_2 from 1σ Fitting Uncertainties for a Typical Arctic Spring Retrieval

Altitude (km)	O_3 Slant Column (molecules/cm^2)	O_3 Profile (ppmv)	NO_2 Slant Column (molecules/cm^2)	NO_2 Profile (ppbv)
50	2.0×10^{17}	1	3.5×10^{15}	0.6
40	3.0×10^{17}	0.06	1.0×10^{15}	0.1
30	4.0×10^{17}	0.03	1.0×10^{15}	0.09
20	2.5×10^{18}	0.06	2.0×10^{15}	0.01
10	1.5×10^{19}	0.003	2.0×10^{16}	0.04

those altitudes. These uncertainty estimates are derived from the 1σ slant column fitting errors (and therefore will vary somewhat from occultation to occultation), but there are also additional uncertainties in the absolute accuracy from model parameter errors. For ozone, the dominant model parameter errors are from the ozone cross-section uncertainty (~2% Ref. 22) and from not accounting for temperature effects in the Chappuis band cross sections (<1%). For NO_2, the dominant model parameter errors are from uncertainties in absolute NO_2 cross sections (<2%, Ref. 22) and the v1.2 retrieval algorithm's neglect of cross-section temperature effects (5%–10%).

As Fig. 10 illustrates, ozone retrievals from the VIS spectrometer tend to agree much better with the FTS and are more reliable than those retrieved from the UV spectrometer at higher altitudes. Kar *et al.* [16] used statistical comparisons to show MAESTRO VIS ozone profiles agree with coincident ozonesonde measurements to within 5%–10% from 16–28 km and with FTS ozone profiles to within 5%–15% from 16 to 50 km. The UV spectrometer retrievals in the wing of the Chappuis band do provide information at lower tangent altitudes, and, in fact, retrieval noise for UV ozone is approximately 0%–25% better than that of the VIS retrievals at altitudes less than 30 km; while above these altitudes, the retrieval noise increases quickly with altitude and UV retrievals become unreliable. Preliminary comparisons between the UV and VIS ozone retrievals indicate agreement within 10% between altitudes of 15–30 km, with the UV ozone exhibiting a low bias. Most importantly, the UV ozone profiles can provide reassurance of the validity of high-vertical-resolution features observed in the VIS ozone profiles.

As can be seen in occultations ss2856 and ss4043, occasional oscillations can be observed in MAESTRO profiles at high altitude and particularly in NO_2. These result from the use of a nonlinear relaxation retrieval that does not apply any auxiliary constraints, such as the use of an *a priori* profile or a smoothing constraint, in a measurement regime where noise is becoming an important issue. The low NO_2 signal at these altitudes is also a factor for the FTS. While FTS ozone profiles are retrieved from ~5 to 95 km, FTS NO_2 is only retrieved from approximately 13–50 km. Kar *et al.* [16] find MAESTRO NO_2 profiles agree with the FTS to within 10%–15%

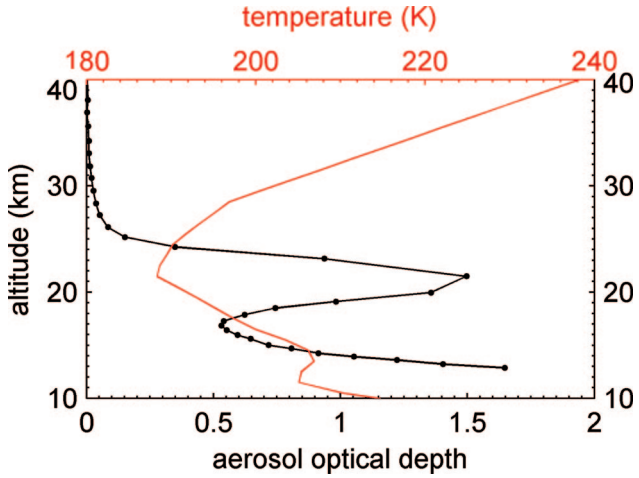

Fig. 11. Total line-of-sight MAESTRO aerosol optical depth at 780 nm for each observed spectrum (black curve with marker at tangent height) for sunrise occultation sr7948 (2 February 2005, 08:06:05 UT at 65.6 °N, 13.4 °E), as well as the ACE *a priori* temperature profile for this location (plain red line), based on the Canadian Meteorological Centre analyses.

from 15 to 40 km (sunrises) and from 22 to 35 km (sunsets).

Although aerosol data products are not included in the v1.2 MAESTRO data, the analysis of aerosol optical depth is under development. Figure 11 shows the detection of a polar stratospheric cloud during sunrise occultation sr7948 (2 February 2005, 08:06:05 UT at 65.6 °N, 13.4 °E), and demonstrates the ability of MAESTRO measurements to resolve vertical structure such as these cloud layers. Figure 11 shows the total aerosol optical depth at 780 nm, just outside the O_2 *A* band, along the MAESTRO line of sight. A prominent optical depth feature from a polar stratospheric cloud is clearly visible, with a peak at 21.5 km and a vertical extent that exceeds the MAESTRO vertical resolution. The temperature profile also reaches a minimum temperature of 188.5 K at precisely this altitude.

6. Data Availability

MAESTRO version 1.2 data (ozone and NO_2 profiles, and wavelength-dependent optical depth) are available from the ACE Science Operations Centre by web access on request to the MAESTRO Principal Investigator (C. T. McElroy) or the Mission Scientist (P. F. Bernath).

7. Conclusions

MAESTRO was launched on SCISAT with the ACE-FTS as part of the Atmospheric Chemistry Experiment on 12 August 2003. As of mid-January 2007, it had observed more than 15,000 solar occultation sunrises and sunsets, as well as several hundred backscatter observations of the Earth's atmosphere. Version 1.2 of MAESTRO data has been released and consists of ozone and NO_2 profiles from occultation measurements, as well as wavelength-dependent optical depth atmospheric extinction. Future versions of

MAESTRO data releases will implement global fitting retrievals, as well as provide results for H_2O- and O_2-derived pressure and temperature [23], and aerosol information separated from the total wavelength dependent optical depth. Eventually, the ACE team hopes to provide a single ozone product for the mission derived by combining information from the FTS and MAESTRO.

This first flight of a UV-VIS-NIR instrument (MAESTRO) and a mid-IR instrument (ACE-FTS) measuring along the same line-of-sight promises to improve our understanding of ozone and NO_2 retrievals in the UV-VIS-NIR and mid-IR, and provide synergistic opportunities for science. In addition, with the recent decommissioning of SAGE II, SAGE III, and POAM III, MAESTRO remains the only primarily solar occultation UV-VIS-NIR instrument in orbit, and is helping to ensure the continuity of important UV-VIS-NIR solar occultation measurements.

The Atmospheric Chemistry Experiment (ACE) is a Canadian-led mission mainly supported by the Canadian Space Agency. The MAESTRO instrument was developed with additional financial support from Environment Canada, the Canadian Foundation for Climate and Atmospheric Sciences, and the Natural Sciences and Engineering Research Council of Canada. Launch services were provided by NASA. The instrument was developed and built by Environment Canada and EMS Technologies. We thank the members of the MAESTRO test team, particularly Ron Irvine, Bob Hum, Paul Chen, and Oleg Mikhailov, for their work during instrument development and preflight characterization.

References

1. P. F. Bernath, C. T. McElroy, M. C. Abrams, C. D. Boone, M. Butler, C. Camy-Peyret, M. Carleer, C. Clerbaux, P.-F. Coheur, R. Colin, P. DeCola, M. De Mazière, J. R. Drummond, D. Dufour, W. F. J. Evans, H. Fast, D. Fussen, K. Gilbert, D. E. Jennings, E. J. Llewellyn, R. P. Lowe, E. Mahieu, J. C. McConnell, M. McHugh, S. D. McLeod, R. Michaud, C. Midwinter, R. Nassar, F. Nichitiu, C. Nowlan, C. P. Rinsland, Y. J. Rochon, N. Rowlands, K. Semeniuk, P. Simon, R. Skelton, J. J. Sloan, M.-A. Soucy, K. Strong, P. Tremblay, D. Turnbull, K. A. Walker, I. Walkty, D. A. Wardle, V. Wehrle, R. Zander, and J. Zou, "Atmospheric Chemistry Experiment (ACE): mission overview," Geophys. Res. Lett. **32,** L15S01, doi:10.1029/2005GL022386 (2005).
2. K. L. Gilbert, D. N. Tumbull, K. A. Walker, C. D. Boone, S. D. McLeod, M. Butler, R. Skelton, P. F. Bernath, F. Chateauneuf, and M.-A. Soucy, "The on-board imagers for the Canadian ACE SCISAT-1 mission" (submitted to J. Geophys. Res.).
3. World Meteorological Organization, *Scientific Assessment of Ozone Depletion: 2002,* Global Ozone and Research Monitoring Project, Report 47 (World Meteorological Organization, 2003).
4. L. W. Thomason and G. Taha, "SAGE III aerosol extinction measurements: initial results," Geophys. Res. Lett. **30,** 1631, doi:10.1029/2003GL017317 (2003).
5. R. L. Lucke, D. R. Korwan, R. M. Bevilacqua, J. S. Hornstein, E. P. Shettle, D. T. Chen, M. Daehler, J. D. Lumpe, M. D. Fromm, D. Debrestian, B. Neff, M. Squire, G. König-Langlo, and J. Davies, "The Polar Ozone and Aerosol Measurement (POAM) III instrument and early validation results," J. Geophys. Res. **104,** 18785–18799 (1999).
6. J. M. Russell III, L. L. Gordley, J. H. Park, S. R. Drayson, W. D. Hesketh, R. J. Cicerone, A. F. Tuck, J. E. Frederick, J. E. Harries, and P. J. Crutzen, "The Halogen Occultation Experiment," J. Geophys. Res. **98,** 10777–10797 (1993).
7. C. D. Boone, R. Nassar, K. A. Walker, Y. Rochon, S. D. McLeod, C. P. Rinsland, and P. F. Bernath, "Retrievals for the atmospheric chemistry experiment Fourier-transform spectrometer," Appl. Opt. **44,** 7218–7231 (2005).
8. C. T. McElroy, "A spectroradiometer for the measurement of direct and scattered solar spectral irradiance from on-board the NASA ER-2 high-altitude research aircraft," Geophys. Res. Lett. **22,** 1361–1364 (1995).
9. C. T. McElroy, C. Midwinter, D. V. Barton, and R. B. Hall, "A comparison of J-values from the composition and photodissociative flux measurement with model calculations," Geophys. Res. Lett. **22,** 1365–1368 (1995).
10. J. P. Burrows, M. Weber, M. Buchwitz, V. Rozanov, A. Ladstätter-Weissenmayer, A. Richter, R. DeBeek, R. Hoogen, K. Bramstedt, K.-U. Eichmann, M. Eisinger, and D. Perner, "The Global Ozone Monitoring Experiment (GOME): mission concept and first scientific results," J. Atmos. Sci. **56,** 151–175 (1999).
11. R. W. Wood, "Anomalous diffraction gratings," Phys. Rev. **48,** 928–936 (1935).
12. D. G. Dufour, J. R. Drummond, C. T. McElroy, C. Midwinter, P. F. Bernath, K. A. Walker, W. F. J. Evans, E. Puckrin, and C. Nowlan, "Intercomparison of simultaneously obtained infrared (4.8 μm) and visible (515–715 nm) ozone spectra using ACE-FTS and MAESTRO," J. Phys. Chem. A **109,** 8760–8764 (2005).
13. D. G. Dufour, J. R. Drummond, C. T. McElroy, C. Midwinter, P. F. Bernath, K. A. Walker, and C. Nowlan, "Simultaneous measurements of visible (400–700 nm) and infrared (3.4 μm) NO_2 absorption," J. Phys. Chem. A **110,** 12414–12418 (2006).
14. L. S. Rothman, D. Jacquemart, A. Barbe, D. C. Benner, M. Birk, L. R. Brown, M. R. Carleer, C. Chackerian Jr., K. Chance, L. H. Coudert, V. Dana, V. M. Devi, J.-M. Flaud, R. R. Gamache, A. Goldman, J.-M. Hartmann, K. W. Jucks, A. G. Maki, J.-Y. Mandin, S. T. Massie, J. Orphal, A. Perrin, C. P. Rinsland, M. A. H. Smith, J. Tennyson, R. N. Tolchenov, R. A. Toth, J. Vander Auwera, P. Varanasi, and G. Wagner, "The HITRAN 2004 molecular spectroscopic database," J. Quant. Spectrosc. Radiat. Transfer **96,** 139–204 (2005).
15. G. L. Thuillier, L. Floyd, T. N. Woods, R. Cebula, E. Hilsenrath, M. Hersé, and D. Labs, "Solar irradiance reference spectra," in *Solar Variability and its Effects on Climate, Geophysical Monograph 141,* J. M. Pap and P. Fox, eds. (American Geophysical Union, 2004), pp. 171–194.
16. J. Kar, C. T. McElroy, J. R. Drummond, J. Zou, F. Nichitiu, K. A. Walker, C. E. Randall, C. R. Nowlan, D. G. Dufour, C. D. Boone, P. F. Bernath, C. R. Trepte, L. W. Thomason, and C. McLinden, "Initial comparison of ozone and NO_2 profiles from ACE-MAESTRO with balloon and satellite data" (submitted to J. Geophys. Res.).
17. M. Carlotti, "Global-fit approach to the analysis of limb-scanning atmospheric measurements," Appl. Opt. **27,** 3250–3254 (1988).
18. J. P. Burrows, A. Richter, A. Dehn, B. Deters, S. Himmelmann, S. Voigt, and J. Orphal, "Atmospheric remote-sensing reference data from GOME—2. Temperature-dependent absorption cross sections of O_3 in the 231–794 nm range," J. Quant. Spectrosc. Radiat. Transfer **61,** 509–517 (1999).
19. J. P. Burrows, A. Dehn, B. Deters, S. Himmelmann, A. Richter, S. Voigt, and J. Orphal, "Atmospheric remote-sensing reference data from GOME: Part 1. Temperature-dependent absorption cross-sections of NO_2 in the 231–794 nm range," J. Quant. Spectrosc. Radiat. Transfer **60,** 1025–1031 (1998).

20. G. D. Greenblatt, J. J. Orlando, J. B. Burkholder, and A. R. Ravishankara, "Absorption measurements of oxygen between 330 and 1140 nm," J. Geophys. Res. **95,** 18577–18582 (1990).
21. M. T. Chahine, "Inverse problems in radiative transfer: determination of atmospheric parameters," J. Atmos. Sci. **27,** 960–967 (1970).
22. J. Orphal and K. Chance, "Ultraviolet and visible absorption cross-sections for HITRAN," J. Quant. Spectrosc. Radiat. Transfer **82,** 491–504 (2003).
23. C. R. Nowlan, "Atmospheric temperature and pressure measurements from the ACE-MAESTRO Space Instrument," Ph.D. dissertation (University of Toronto, 2006).